Dalton Transactions

PAPER

View Article Online
View Journal | View Issue

Cite this: *Dalton Trans.*, 2017, **46**, 14021

A new glance on R_2MGe_6 (R = rare earth metal, M = another metal) compounds. An experimental and theoretical study of R_2PdGe_6 germanides†

Riccardo Freccero, [a] Pavlo Solokha, *[a] Davide M. Proserpio, [b,c] Adriana Saccone [a] and Serena De Negri [a]

The R_2PdGe_6 series (R = rare earth metal) was structurally characterized, and the results achieved were extended for a comprehensive study on R_2MGe_6 (M = another metal) compounds, employing symmetry-based structural rationalization and energy calculations. Directly synthesized R_2PdGe_6 exists for almost all R-components (R = Y, La–Nd, Sm and Gd–Lu) and even if with La is probably metastable. Several single crystal X-ray analyses (R = Y, Ce, Pr, Nd, Er and Lu) indicated *oS*72-$Ce_2(Ga_{0.1}Ge_{0.9})_7$ as the correct structure. The alternative In-flux method, once optimized, produced three good quality R_2PdGe_6 single crystals: La_2PdGe_6 and Pr_2PdGe_6 turned out to be *mS*36-La_2AlGe_6-type non-merohedrally twinned crystals and Yb_2PdGe_6 is of *oS*72-$Ce_2(Ga_{0.1}Ge_{0.9})_7$-type. The vacancy ordering phenomenon was considered as a possible cause of the symmetry reduction relations connecting the most frequently reported 2 : 1 : 6 structural models (*oS*18, *oS*72 and *mS*36) with the *oS*20-$SmNiGe_3$ aristotype. The detected twin formation is consistent with the symmetry relations, which are discussed even considering the validity of the different structural models. DFT total energy calculations were performed for R_2PdGe_6 (R = Y and La) in the three abovementioned structural models, and for La_2MGe_6 (M = Pt, Cu, Ag and Au) in the *oS*18 and *oS*72 modifications. The results indicate that the *oS*18-Ce_2CuGe_6 structure, prevalently proposed in the literature, is associated with the highest energy and thus it is not likely to be realized in these series. The *oS*72 and *mS*36 polytypes are energetically equivalent, and small changes in the synthetic conditions could easily stabilize any of them, in agreement with experimental results obtained by direct and flux syntheses.

Received 23rd July 2017,
Accepted 18th September 2017

DOI: 10.1039/c7dt02686b

rsc.li/dalton

1. Introduction

Numerous germanium-rich compounds of idealized general formula R_2MGe_6 (R = rare earth metal, M = another metal) have been investigated since the eighties of the last century up to the present.[1] Some R_2MGe_6 are off-stoichiometric due to the M/Ge statistical mixture (as in $Ce_2(Ga_{0.1}Ge_{0.9})_7$) or to partially occupied M sites (as in $Dy_2Zn_{1-x}Ge_6$ ($x \sim 0.5$)[2]). Scientific interest in these phases arises from the fact that they exist with many different metals M, ranging from the s-block (M = Li and Mg) to the p-block (M = Al and Ga) of the periodic table, including the major part of late transition elements. For this reason, title compounds are well suited for systematic studies on crystal structure–electronic structure–property relationships, aiming to evidence for example the role of both R and M properties (size, electronegativity, valence electrons, *etc.*) in the chemical bonding scenario, set up by characteristic Ge-based covalent fragments.

A variety of physical properties, including electrical resistivity, magnetic susceptibility, specific heat and thermoelectric power, have already been measured on several R_2MGe_6 representative samples, mostly with transition elements, such as Co, Ni, Pd, Pt and Cu, as M components.[3–9]

Many of the investigated compounds exhibit an antiferromagnetic ordering below ~30 K;[3,4,8] for some Yb_2MGe_6 phases a behaviour characteristic of intermediate valence systems has been reported.[5,9,10]

Despite the great amount of experimental work, controversial data exist both on the interpretation of the physical/magnetic properties and on the crystal structures of the R_2MGe_6

[a]*Università di Genova, Dipartimento di Chimica e Chimica Industriale, Via Dodecaneso 31, 16146 Genova, Italy. E-mail: pavlo.solokha@unige.it; Fax: +39-0103536163; Tel: +39-0103536159*
[b]*Università degli Studi di Milano, Dipartimento di Chimica, Via Golgi 19, 20133 Milano, Italy*
[c]*Samara Center for Theoretical Materials Science (SCTMS), Samara State University, Ac. Pavlov Str. 1, Samara 443011, Russia*

†Electronic supplementary information (ESI) available: X-ray crystallographic files in CIF format; back scattered electron images of alloy surfaces; summary of attempts to synthesize the La_2PdGe_6 compound; calculated X-ray powder patterns; interatomic distances obtained by single crystal X-ray analysis. See DOI: 10.1039/c7dt02686b

compounds. They are generally reported to crystallize in orthorhombic or monoclinic space groups, distributing among the following prototypes: *oS*18-Ce_2CuGe_6 (space group: *Amm*2), which is the most represented, *oS*72-$Ce_2(Ga_{0.1}Ge_{0.9})_7$ (space group: *Cmce*) and *mS*36-La_2AlGe_6 (*C*2/*m*). A different orthorhombic structure (space group: *Cmmm*) has been assigned to a few R_2LiGe_6 (R = La, Ce and Pr) phases, referred to as the *oS*18-Pr_2LiGe_6 prototype[11,12] and to $Yb_2Pd_{1.075(1)}Ge_6$, referred to as the *oS*20-$SmNiGe_3$ prototype.[13]

The *oS*72-$Ce_2(Ga_{0.1}Ge_{0.9})_7$ structure was found to be the correct one for a number of compounds previously reported as *oS*18, such as La_2PdGe_6, Dy_2PdGe_6 [7,14] and Yb_2PdGe_6,[9,15] and for several new 2 : 1 : 6 representative samples, such as La_2MgGe_6 [16] and R_2ZnGe_6.[2] Interestingly, along the Zn-containing series of compounds, a structural change was observed from the orthorhombic *oS*72-$Ce_2(Ga_{0.1}Ge_{0.9})_7$ structure (R = La–Nd, Sm, Gd and Tb) to the new monoclinic structure *mP*34-$Dy_2Zn_{1-x}Ge_6$ ($x \sim 0.5$, R = Dy and Ho), which is an ordered superstructure of the La_2AlGe_6 prototype.

Recently, the alternative synthesis in metal flux was employed for Yb_2CuGe_6, and the *mS*36-La_2AlGe_6 crystal structure was proposed for this compound, instead of the previously reported *oS*18-Ce_2CuGe_6 type.[17]

The abovementioned structural models *oS*18, *oS*72 and *mS*36 are strictly related, as can be pointed out both by means of group–subgroup relations[2] and by a description based on the linear intergrowth concept.[18,19] As a consequence, the correct model can be assigned only by single crystal X-ray diffraction analysis; powder X-ray diffraction could be sufficient only in the case of high quality patterns of single phase samples, generally quite difficult to obtain.

A correct structural description is of fundamental importance not only to evidence differences, similarities and regularities among the numerous 2 : 1 : 6 compounds in view of further chemical bonding studies, but also to appropriately interpret the results of magnetic characterization.

Taking into account the fact that the R_2PdGe_6 phases are reported to exist for many rare earth metals and that the structures of some of them were recently revised, this 2 : 1 : 6 series of compounds were targeted to perform an accurate structural investigation, mostly based on single crystal analysis.

The challenging experimental work necessary for this achievement was complemented both by a comprehensive crystal structure analysis based on group–subgroup relations and by DFT total energy calculations, in order to generalize the obtained results to the whole R_2MGe_6 family and guide future investigations on new compounds.

2. Experimental section

2.1 Synthesis, microstructure and phase analysis

Different synthetic routes were followed, all starting from the pure components (rare earth metals and In used as a metal solvent were supplied by Newmet Koch, Waltham Abbey, England, palladium and germanium by MaTecK, Jülich, Germany, nominal purities of all metals >99.9 mass %).

Samples of about 0.8 g with $R_{22.2}Pd_{11.1}Ge_{66.7}$ (R = Sc; Y; La–Nd; and Sm–Lu) nominal compositions were prepared by direct synthesis in a resistance furnace. Stoichiometric amounts of components were placed in an arc-sealed Ta crucible in order to prevent oxidation; the constituents of the $Eu_{22.2}Pd_{11.1}Ge_{66.7}$ sample were weighed and sealed in the crucible inside an inert atmosphere glove box. The Ta crucible was then closed in an evacuated quartz phial to prevent oxidation at high temperature, and finally placed in a resistance furnace, where the following thermal cycle was employed:

$$25\ ^\circ\mathrm{C} \rightarrow (10\ ^\circ\mathrm{C\ min^{-1}}) \rightarrow 950\ ^\circ\mathrm{C} \rightarrow (-0.2\ ^\circ\mathrm{C\ min^{-1}}) \rightarrow 350\ ^\circ\mathrm{C} \rightarrow \text{furnace switched off} \quad \text{(I)}$$

A continuous rotation, at a speed of 100 rpm, was applied to the phial during the thermal cycle. These synthetic conditions were chosen with the aim to obtain samples containing crystals of good quality and size, suitable for further structural studies. The synthesized alloys are very brittle and mostly stable in air, except for the $Eu_{22.2}Pd_{11.1}Ge_{66.7}$ sample. No tantalum contamination of the samples was detected.

After direct synthesis in the resistance furnace, some pieces of the $La_{22.2}Pd_{11.1}Ge_{66.7}$ sample were annealed at different temperatures. Further attempts to synthesize the La_2PdGe_6 compound were made, by arc melting of components, followed by annealing treatments (see the "Results and discussion" section).

Flux synthesis was also performed for samples containing La, Pr and Yb, using In as a metal solvent. Stoichiometric amounts of R, Pd and Ge, giving the nominal composition of $R_{21}Pd_7Ge_{72}$, were placed in an arc-sealed Ta crucible with a 1 : 45 molar excess of indium, to obtain a total mass of about 3 g. Then, the Ta crucible, closed in an evacuated quartz phial, was placed in a resistance furnace, and the following thermal cycles were employed:

$$25\ ^\circ\mathrm{C} \rightarrow (2\ ^\circ\mathrm{C\ min^{-1}}) \rightarrow 1000\ ^\circ\mathrm{C}\ (5\ \mathrm{h}) \rightarrow (-1.0\ ^\circ\mathrm{C\ min^{-1}}) \rightarrow 850\ ^\circ\ \mathrm{C}(48\ \mathrm{h}) \rightarrow (-0.3\ ^\circ\mathrm{C\ min^{-1}}) \rightarrow 25\ ^\circ\mathrm{C} \quad \text{(II)}$$

$$25\ ^\circ\mathrm{C} \rightarrow (10\ ^\circ\mathrm{C\ min^{-1}}) \rightarrow 750\ ^\circ\mathrm{C}\ (24\ \mathrm{h}) \rightarrow (-0.5\ ^\circ\mathrm{C\ min^{-1}}) \rightarrow 25\ ^\circ\mathrm{C} \quad \text{(III)}$$

For the La-containing sample both thermal cycles were tested, but only cycle III was employed for the Pr and Yb-containing samples.

A continuous rotation of the quartz phial during the thermal cycle was employed to favour better dissolution of the constituting elements inside the flux. In all cases, a vertical section of the obtained ingots revealed the presence of large shining crystals, visible to the naked eye, randomly distributed within the flux solidified matrix.

In order to perform metallographic analysis, samples were embedded in a phenolic resin with a carbon filler by using the automatic hot compression mounting press Opal 410

(ATM GmbH, Germany). The samples synthesized by the flux method were analysed prior to product separation: to avoid the metal solvent melting, they were embedded in a cold-curing resin, conductive due to the presence of a copper filler.

The automatic grinding and polishing machine Saphir 520 (ATM GmbH, Germany) was used to obtain smooth alloy surfaces suitable for microscopic examinations. Grinding was performed using SiC papers with grain size decreasing from 600 to 1200 mesh, using running water as a lubricant; for polishing, diamond paste with particle size decreasing from 6 to 1 μm was used with an alcohol based lubricant. Petroleum ether was employed to clean samples ultrasonically after each polishing step.

In the case of flux prepared samples only the 1200 mesh SiC paper was used applying a low pressure, due to In ductility.

After SEM-EDXS analysis, crystals of R_2PdGe_6 compounds (R = La, Pr and Yb) obtained by flux synthesis were extracted from the flux by immersion and sonication of the ingot in glacial acetic acid for about 24 h, allowing indium dissolution. The obtained crystalline product was rinsed with water and dried with acetone. After that, another SEM-EDXS analysis was performed in order to check the goodness of the separation procedure and the quality/composition of the isolated crystals.

Microstructure examination as well as qualitative and quantitative analyses were performed using a scanning electron microscope (SEM) Zeiss Evo 40 (Carl Zeiss SMT Ltd, Cambridge, England) equipped with a Pentafet Link Energy Dispersive X-ray Spectroscopy (EDXS) system managed using INCA Energy software (Oxford Instruments, Analytical Ltd, Bucks, UK). Cobalt standard was used for calibration.

2.2 X-ray diffraction (XRD) analysis on single crystal and powder samples

Single crystals of R_2PdGe_6 compounds prepared by both direct synthesis (R = Y, Ce, Pr, Nd, Er and Lu) and flux synthesis (R = La, Pr and Yb) were selected with the aid of a light optical microscope (Leica DM4000 M, Leica Microsystems Wetzlar GmbH, Wetzlar, Germany) operated in the dark field mode.

A full-sphere dataset was obtained in a routine fashion under ambient conditions on a four-circle Bruker Kappa APEXII CCD area-detector diffractometer equipped with graphite monochromatized Mo Kα (λ = 0.71073 Å) radiation, operating in ω-scan mode. Crystals exhibiting metallic luster, glued on glass fibres, were mounted in a goniometric head and then in the goniostat inside the diffractometer camera. Intensity data were collected over the reciprocal space up to ~30° in θ with exposures of 20–30 s per frame. Semiempirical absorption corrections based on a multipolar spherical harmonic expansion of equivalent intensities were employed for all data using SADABS/TWINABS software.[20]

The details of the crystal structure solution and refinement are reported in the "Results and discussion" section. The corresponding CIF files are available in the ESI† and they have also been deposited at Fachinformationszentrum Karlsruhe, 76344 Eggenstein-Leopoldshafen, Germany, with the following depository numbers: CSD 433026 (Y_2PdGe_6), CSD 433022 (La_2PdGe_6, flux), CSD 433081 (Ce_2PdGe_6), CSD 433025 (Pr_2PdGe_6), CSD 433205(Pr_2PdGe_6, flux), CSD 433024 (Nd_2PdGe_6), CSD 433021 (Er_2PdGe_6), CSD 433151 (Yb_2PdGe_6, flux), CSD 433023 (Lu_2PdGe_6).

Selected crystallographic data and structure refinement parameters for the studied single crystals are listed in Tables 1 and 2.

X-ray powder diffraction (XRPD) was performed on all samples by using a diffractometer Philips X'Pert MPD (Cu Kα radiation, λ = 1.5406 Å, graphite crystal monochromator, scintillation detector, step mode of scanning), with a θ:2θ Bragg–Brentano geometry. Measured powder patterns were collected in the 10°–100°2θ range, with a scanning step of *ca.* 0.02° with a time per step varying from 10 to 20 s. Phase identification was performed with the help of the software PowderCell.[21]

2.3 Differential thermal analysis (DTA)

Differential thermal analysis (DTA) was performed on a few La–Pd–Ge samples, in order to gain insights into the formation conditions of the La_2PdGe_6 compound. Measurements were carried out using a LABSYS EVO (SETARAM Instrumentation, Caluire, France) equipped with type S (Pt–PtRh 10%) thermocouples, in the temperature range of 25–1100 °C using custom-made tantalum crucibles. The sample crucible was loaded with about 200 mg of the alloy to analyze, closed with a cap, and subsequently arc-sealed under an inert atmosphere after cooling it in liquid nitrogen, so as to avoid undesired reactions. A crucible of the same weight as the sample container was used as the reference. The DTA curves were recorded under a continuous flow of argon (20 mL min^{-1}) to avoid oxidation of the crucibles at high temperatures. Different thermal cycles were employed depending on the sample. The obtained thermograms were evaluated with the software Calisto, supplied by SETARAM with the DTA equipment. Prior and after the DTA experiments the samples were characterized by SEM/EDXS and/or XRPD.

2.4 Computational details

DFT total energy calculations were performed for R_2PdGe_6 (R = Y and La) in the three structural modifications *oS*18, *oS*72 and *mS*36, and for La_2MGe_6 (M = Pt, Cu, Ag and Au) in the two orthorhombic modifications, by means of the plane wave pseudopotential code QUANTUM-ESPRESSO.[22] The PBE functional[23] for the exchange and correlation energy was used. Ultrasoft pseudopotentials,[24] available in the "GBRV" open-source library,[25] were employed for M, La and Y, whereas for Ge a norm-conserving pseudopotential, including the 4s and 4p valence orbitals, was used. The semicore states 4p for Pd, 5p for Pt, 3s and 3p for Cu, 4s and 4p for Ag and Y and 5s and 5p for La were treated as valence electrons. The Brillouin zone was sampled within uniform grids generated with different *k*-points for the three polymorphs: 12 × 12 × 2 for the *oS*18 modification, 6 × 6 × 2 for *oS*72 and 6 × 6 × 4 for *mS*36. The plane-wave and density cut-off were set to 45 Ry and 450 Ry, respectively. The orbital occupancies at the Fermi level were treated with a Gaussian smearing of 0.01 Ry.

Table 1 Crystallographic data for R_2PdGe_6 (R = Y, Ce, Pr, Nd, Er and Lu) single crystals taken from samples prepared by direct synthesis and experimental details of the structural determination. All compounds are isostructural (space group: *Cmce*, No. 64; Pearson's symbol-prototype: oS72-$Ce_2(Ga_{0.1}Ge_{0.9})_7$; Z = 8)

Empirical formula	Y_2PdGe_6	Ce_2PdGe_6	Pr_2PdGe_6	Nd_2PdGe_6	Er_2PdGe_6	Lu_2PdGe_6
EDXS data	$Y_{21.0}Pd_{10.8}Ge_{68.2}$	$Ce_{22.2}Pd_{10.8}Ge_{67.0}$	$Pr_{20.2}Pd_{11.4}Ge_{68.4}$	$Nd_{21.8}Pd_{11.2}Ge_{67.0}$	$Er_{22.7}Pd_{11.0}Ge_{66.3}$	$Lu_{23.8}Pd_{10.6}Ge_{65.6}$
M_w, [g mol^{-1}]	719.76	822.18	823.76	830.42	876.46	891.88
a [Å]	8.1703(5)	8.3548(4)	8.3129(5)	8.2831(4)	8.1122(6)	8.0725(8)
b [Å]	8.0451(5)	8.1774(4)	8.1540(5)	8.1323(4)	8.0068(6)	7.9791(8)
c [Å]	21.558(1)	22.0272(9)	21.996(1)	21.915(1)	21.399(2)	21.317(2)
V [Å^3]	1417.1(2)	1504.9(1)	1491.0(2)	1476.2(1)	1389.9(2)	1373.0(2)
Calc. density [g cm^{-3}]	6.748	7.258	7.340	7.473	8.377	8.629
Abs. coeff. (μ), mm^{-1}	43.6	37.7	38.9	40.1	51.8	56.8
Unique reflections	1028	1308	1296	1307	1206	1225
Reflections $I > 2\sigma(I)$	884	1072	870	848	1020	874
R_{sigma}	0.0233	0.0084	0.0270	0.0263	0.0133	0.0284
Data/parameters	884/50	1072/50	870/50	848/50	1020/50	874/50
GOF on F^2 (S)	1.166	1.543	1.059	1.002	1.326	0.912
R indices [$I > 2\sigma(I)$]	R_1 = 0.0232; wR_2 = 0.0642	R_1 = 0.0208; wR_2 = 0.0364	R_1 = 0.0197; wR_2 = 0.0372	R_1 = 0.0165; wR_2 = 0.0299	R_1 = 0.0202; wR_2 = 0.0331	R_1 = 0.0224; wR_2 = 0.0557
R indices [all data]	R_1 = 0.0282; wR_2 = 0.0667	R_1 = 0.0260; wR_2 = 0.0379	R_1 = 0.0366; wR_2 = 0.0421	R_1 = 0.0351; wR_2 = 0.0354	R_1 = 0.0264; wR_2 = 0.0343	R_1 = 0.0399; wR_2 = 0.0634
$\Delta\rho_{fin}$ (max/min), [e Å^{-3}]	1.31/−1.36	1.03/−1.29	1.01/−1.68	1.26/−1.05	1.09/−1.25	1.77/−1.63

Table 2 Crystallographic data for R_2PdGe_6 (R = La, Pr and Yb) single crystals taken from samples prepared by flux-synthesis and experimental details of the structural determination

Empirical formula	La_2PdGe_6	Pr_2PdGe_6	Yb_2PdGe_6
EDXS data	$La_{22.4}Pd_{10.5}Ge_{67.1}$	$Pr_{20.6}Pd_{11.3}Ge_{68.1}$	$Yb_{23.2}Pd_{10.9}Ge_{65.9}$
M_w, [g mol^{-1}]	819.76	823.76	888.02
Space group (no.)	*C*2/*m* (12)	*C*2/*m* (12)	*Cmce* (64)
Pearson symbol-prototype, Z	*mS*36-La_2AlGe_6, 4	*mS*36-La_2AlGe_6, 4	*oS*72-$Ce_2(Ga_{0.1}Ge_{0.9})_7$, 8
a [Å]	8.2163(8)	8.157(2)	8.1428(3)
b [Å]	8.4161(9)	8.328(2)	7.9807(3)
c [Å]	11.294(1)	11.195(2)	21.8331(9)
β (°)	100.477(1)	100.391(3)	90
V [Å^3]	768.0(1)	748.1(3)	1418.83(9)
Calc. density [g cm^{-3}]	7.090	7.314	8.314
abs coeff. (μ), mm^{-1}	36.2	38.7	53.5
Twin law	[1 0 0 0 −1 0 −1/2 0 −1]	[1 0 0 0 −1 0 −1/2 0 −1]	—
k(BASF)	0.414(5)	0.423(5)	—
Unique reflections	1083	1262	1242
Reflections $I > 2\sigma(I)$	1030	1062	1144
R_{sigma}	0.0218	0.0298	0.0149
Data/parameters	1030/50	1062/50	1144/50
GOF on F^2 (S)	1.200	1.453	1.428
R indices [$I > 2\sigma(I)$]	R_1 = 0.0242; wR_2 = 0.0773	R_1 = 0.0357; wR_2 = 0.1166	R_1 = 0.0231; wR_2 = 0.0496
R indices [all data]	R_1 = 0.0254; wR_2 = 0.0778	R_1 = 0.0501 wR_2 = 0.1209	R_1 = 0.0255; wR_2 = 0.0506
$\Delta\rho_{fin}$ (max/min), [e Å^{-3}]	2.33/−2.61	4.35/−5.29	1.92/−1.78

3. Results and discussion

3.1 The formation of R_2PdGe_6 germanides along the R series

The results of SEM/EDXS characterization confirm the presence of the R_2PdGe_6 phase in most of the samples prepared by direct synthesis (see Table 3).

According to the SEM micrographs, under the applied experimental conditions for direct synthesis, R_2PdGe_6 is generally the highest yield phase. As it is common for alloys prepared by slow cooling from liquid, many secondary phases were detected, among which $R(Pd,Ge)_{2-x}$, $R_2Pd_3Ge_5$, $RPdGe_2$ and Ge are the most common. Representative microstructures are available in the ESI.†

In samples with R = Sc and Eu no traces of the R_2PdGe_6 phase were detected: in both cases three-phase alloys were obtained, in which an already known ternary compound (ScPdGe or $EuPdGe_3$) coexists with Ge and the binary RGe_{2-x} phase dissolving a small amount of Pd.

In the $La_{22.2}Pd_{11.1}Ge_{66.7}$ sample prepared by direct synthesis employing cycle I (sample code "La" in Table 3), only a small amount of La_2PdGe_6 was found, in the form of a thin border around big $LaGe_{2-x}$ crystals (see Fig. 1a). From such a sample,

Table 3 Results of SEM/EDXS characterization of the $R_{22.2}Pd_{11.1}Ge_{66.7}$ samples prepared by direct synthesis in the resistance furnace using cycle I and of the $R_{21}Pd_7Ge_{72}$ samples prepared by flux synthesis using cycle III (indicated with *f* in the sample code)

Sample code (R)	R_2PdGe_6 phase composition [EDXS, at%] R; Pd; Ge	Other known detected phases		
Sc	–	$Sc(Pd,Ge)_{2-x}$	Ge	ScPdGe
Y[a]	21.0; 10.8; 68.2	$YPdGe_2$		
La	22.4; 9.9; 67.7	$La(Pd,Ge)_{2-x}$	Ge	$LaPdGe_3$
La,[a] *f*	22.4; 10.5; 67.1	$La(Pd,Ge)_{2-x}$	Ge	
Ce[a]	22.5; 10.8; 66.7		Ge	$Ce_2Pd_3Ge_5$
Pr[a]	20.2; 11.4; 68.4		Ge	$Pr_2Pd_3Ge_5$
Pr,[a] *f*	20.7; 11.0; 68.3	$Pr(Pd,Ge)_{2-x}$	Ge	
Nd[a]	21.8; 11.2; 67.0	$NdPdGe_2$	Ge	$Nd_2Pd_3Ge_5$
Sm	21.5; 11.1; 67.4		Ge	$Sm_2Pd_3Ge_5$
Eu	–	$Eu(Pd,Ge)_{2-x}$	Ge	$EuPdGe_3$
Gd	22.2; 11.4; 66.4	$Gd(Pd,Ge)_{2-x}$		
Tb	22.2; 11.1; 66.7	$TbPdGe_2$		
Dy	22.7; 10.9; 66.4	$DyPdGe_2$		
Ho	22.3; 11.3; 66.4	$Ho(Pd,Ge)_{2-x}$		
Er[a]	22.7; 11.0; 66.3	$Er(Pd,Ge)_{2-x}$		
Tm	23.0; 11.1; 65.9	$Tm(Pd,Ge)_{2-x}$		
Yb	23.1; 10.7; 66.2	$Yb(Pd,Ge)_{2-x}$		
Yb,[a] *f*	23.2; 10.9; 65.9	$YbGe_{2-x}$		
Lu[a]	23.8; 10.6; 65.6	$Lu(Pd,Ge)_{2-x}$	Ge	

[a] Samples where single crystals were taken.

it was not possible to isolate suitable single crystals. In the literature, this phase has been reported to crystallize in the *oS*18-Ce_2CuGe_6 [3] or in the *oS*72-$Ce_2(Ga_{0.1}Ge_{0.9})_7$ model,[4] the latter with no complete structural data available. For this reason, further attempts were made to synthesize a La_2PdGe_6 sample convenient for structural resolution, which are briefly accounted for in the following.

The as-cast samples with nominal composition $La_{22.2}Pd_{11.1}Ge_{66.7}$ did not show any trace of La_2PdGe_6, independently using the melting method (arc or induction furnace). These samples are characterized by a clear microstructure, where crystals of $La(Pd,Ge)_{2-x}$ and $LaPdGe_3$ coexist with an eutectic structure containing Ge (see Fig. 1b). Annealing at 700 °C of an as-cast sample for 2 weeks, performed on the basis of literature data,[4] did not succeed in obtaining the desired compound; what is more, the same annealing treatment carried out on the sample (La) prepared using cycle I caused the thin La_2PdGe_6 border to disappear.

At this point, it became clear that La_2PdGe_6 behaves somewhat differently from the other rare earth homologues, and DTA measurements were performed in order to gain insights into its temperature formation.

The DTA curve obtained at a heating rate of 5 °C min^{-1} (T_{max} = 1100 °C), is shown in Fig. S2 (ESI†). Four thermal effects were detected at the following temperatures (onset): 800 °C, 886 °C, 927 °C and 1027 °C. The same thermal effects are recorded on cooling. The peak at 800 °C is in good agreement with the temperature of the binary eutectic equilibrium L → (Ge) + $LaGe_{2-x}$ reported at T = 810 °C.[26] However, the other peaks are not easily interpretable. After this thermal cycle the presence of a small amount of La_2PdGe_6 was indeed detected by SEM-EDXS analysis in the form of a border between $La(Pd,Ge)_{2-x}$ and $LaPdGe_3$ (see Fig. 1c). In a restricted region of the sample after DTA, bigger crystals of La_2PdGe_6 are present enclosing a brighter core of $LaPdGe_3$ (see Fig. 1d). The measured global composition of this region is $La_{21}Pd_7Ge_{72}$. Aiming to obtain a higher yield of the desired compound, different annealing treatments (lasting for one month each) were performed at 830 °C, 890 °C and 1000 °C: temperatures were chosen slightly below the recorded thermal effects. Unfortunately, no traces of 2 : 1 : 6 were found after all these treatments. From the gathered results, it was concluded that La_2PdGe_6 is probably a metastable phase which is likely to form only in small amounts during relatively slow cooling.

It is known that alternative synthetic routes may help to produce metastable compounds; among them, the flux method was targeted, taking into account both literature data[27] and our previous results on related $R_2Pd_3Ge_5$ compounds.[28] As a metal solvent In was chosen considering its ability to dissolve Ge, rare earth and transition metals, without forming In–Ge binary compounds, allowing the formation of ternary phases.[27,29] Thus, several attempts were made varying both the nominal composition and the thermal cycle. Good results were obtained starting from the nominal composition $La_{21}Pd_7Ge_{72}$: the 2 : 1 : 6 phase was obtained using both cycle II and cycle III (see Fig. 1e and f). After cycle II, however, La_2PdGe_6 is almost always found as a grey border of big $La(Pd,Ge)_{2-x}$ crystals and only a few single phase crystals were detected. On the contrary, after cycle III, characterized by a lower maximum temperature (750 °C instead of 1000 °C), many 2 : 1 : 6 single crystals were obtained, allowing further crystal structure determination after their separation from the In-flux (sample indicated by code "La,[a] *f*" in Table 3). More details on all samples prepared with La can be found in the ESI.†

Unexpectedly, the flux synthesized La_2PdGe_6 turned out to be monoclinic, differently from all the other series of samples prepared by direct synthesis (see section 3.2): for this reason the flux method (cycle III) was tested also on $Pr_{21}Pd_7Ge_{72}$ and $Yb_{21}Pd_7Ge_{72}$ samples. In both cases R_2PdGe_6 phases were detected and analysed by X-ray diffraction (see Table 3); particularly good quality big crystals were obtained in the case of R = Yb (see Fig. 2).

3.2 Crystal structure of R_2PdGe_6 (R = Y, La (flux), Ce, Pr, Pr (flux), Nd, Er, Yb(flux) and Lu)

To definitively establish the crystal structure of R_2PdGe_6 only the X-ray powder diffraction data are not sufficient. In fact, differences are hardly visible in the calculated diffraction patterns of the orthorhombic and the monoclinic models (see the ESI†). Additionally, the recognition of the correct model is hampered by the fact that samples are usually multiphase giving strong peak overlaps. Hence, single crystal X-ray diffrac-

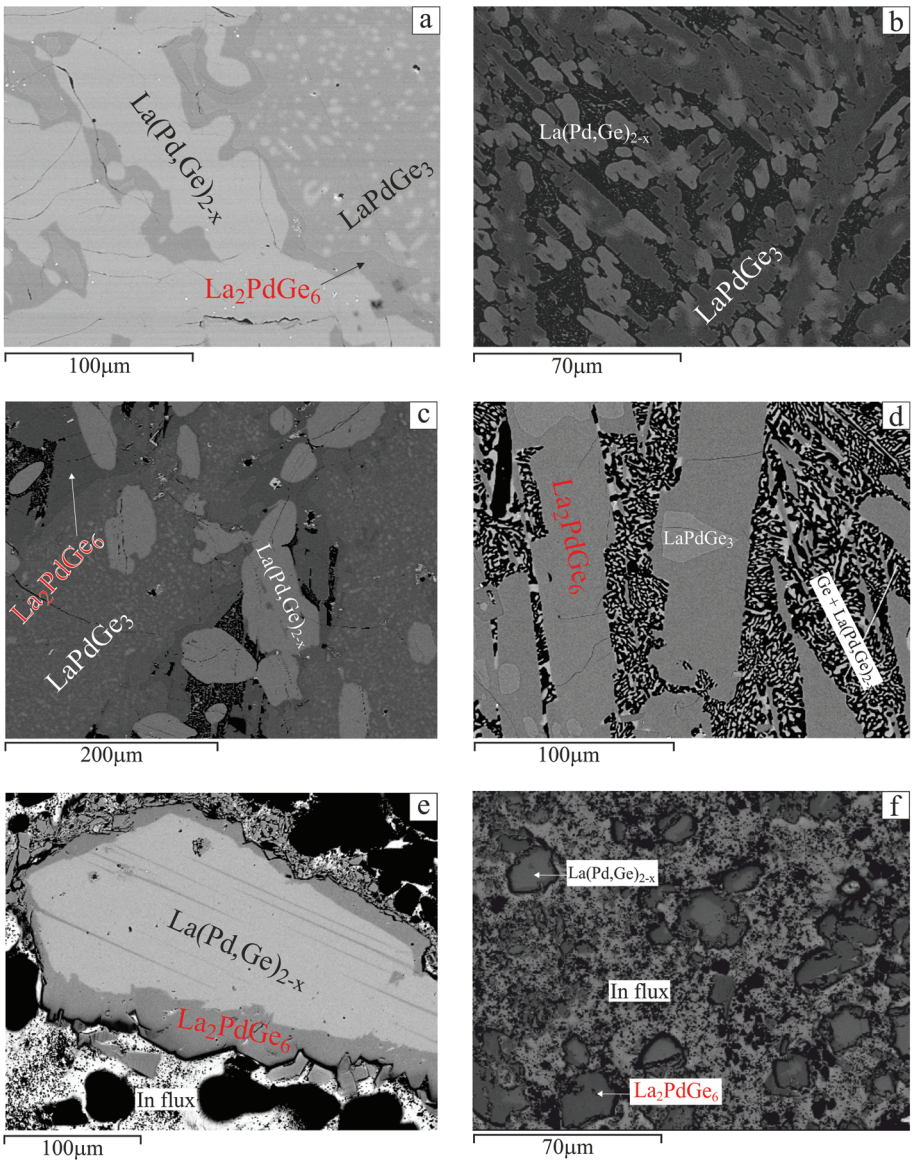

Fig. 1 Micrographs (SEM-BSE mode) of representative samples of $La_{22.2}Pd_{11.1}Ge_{66.7}$ nominal composition (a–d) and of $La_{21}Pd_7Ge_{72}$ nominal composition (e, f) obtained under the following experimental conditions: (a) synthesis in the resistance furnace, cycle I; (b) arc melting; (c, d) arc melting followed by one DTA cycle; (e) synthesis in the resistance furnace with In flux, cycle II; (f) synthesis in the resistance furnace with In flux, cycle III.

tion is the fundamental method used for the structural investigations conducted here.

For single crystals of R_2PdGe_6 (R = Y, Ce, Pr, Nd, Er, Yb(*f*) and Lu) compounds (see. Table 1) the cell indexation was straightforward giving an orthorhombic *C*-centered cell (only $h + k = 2n$ reflections were observed). The analysis of systematic extinctions suggested *Cc*2*e* (no. 41) and *Cmce* (no. 64) as the possible space groups. An almost complete structural model was obtained in the *Cmce* space group in a few iteration cycles by using the charge-flipping algorithm implemented in JANA2006.[30] In this model the rare earth atoms are situated in a 16*g* general site and palladium occupies the 8*f* site, while all the other positions are assigned to the lighter germanium atoms. The obtained models have the *oS*72 Pearson symbol and correspond to the R_2PdGe_6 stoichiometry, satisfactorily matching with the EDXS microprobe analysis data.

The further structure refinements were carried out by full-matrix least-squares methods on $|F^2|$ using the SHELX programs.[31] The site occupancy factors of all species were checked for deficiency, in separate cycles of refinement, obtaining values very close to unity. At this point neither the deficiency nor statistical mixture was considered and stoichiometric R_2PdGe_6 models were further anisotropically refined giving acceptable residuals and flat difference Fourier maps. The results indicate that the Y, Ce, Pr, Er and Lu containing compounds prepared by direct synthesis are isopointal with

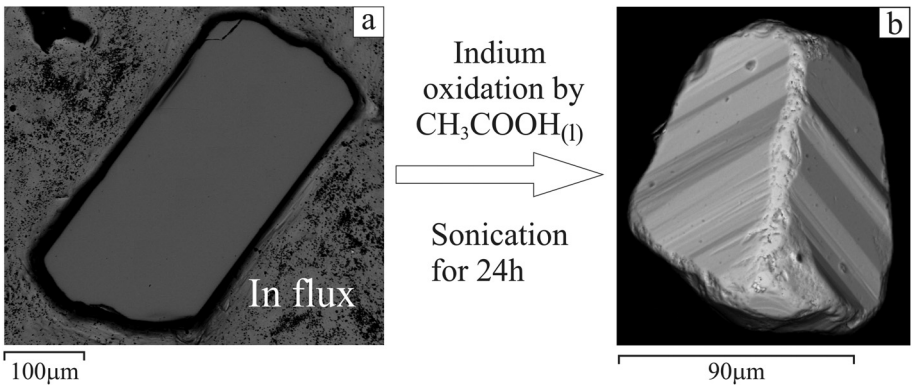

Fig. 2 SEM-BSE micrographs for the Yb_2PdGe_6 single crystal before (a) and after (b) the selective In oxidation.

the $Ce_2(Ga_{0.1}Ge_{0.9})_7$ prototype. The same is true also for the Yb containing compound prepared by flux synthesis (the image of this crystal is reported in Fig. 2).

The atomic positions of the R_2PdGe_6 compounds are listed in Table 4 together with the equivalent isotropic displacement parameters. The positions were standardized with the Structure Tidy program.[32] The interatomic distances are available in the ESI.†

The La_2PdGe_6 crystal selected for X-ray analysis, taken from a flux synthesized sample, is an example of a non-merohedral twin composed of two domains of comparable dimensions. Normally, twins of such a type have problems in the preliminary stages of cell indexing (leading to unexpectedly high values of unit cell parameters) and space group determination (showing inconsistency with any known space group systematic absence).[33,34] Instead, in our case the unit cell indexing was

Table 4 Atomic coordinates and equivalent isotropic displacement parameters (Å^2) for the studied R_2PdGe_6 single crystals with the *oS*72-$Ce_2(Ga_{0.1}Ge_{0.9})_7$ crystal structure

Atom (site)	Atomic param.	R = Y	R = Ce	R = Pr	R = Nd	R = Er	R = Yb (*f*)	R = Lu
R	*x*/*a*	0.25102(5)	0.25042(2)	0.25041(2)	0.25049(2)	0.25120(2)	0.24952(3)	0.25159(3)
(16*g*)	*y*/*b*	0.37584(5)	0.37513(5)	0.3753(1)	0.3751(1)	0.37605(3)	0.37604(3)	0.37592(4)
	z/*c*	0.08125(2)	0.08270(2)	0.082540(9)	0.082326(8)	0.080953(8)	0.08257(2)	0.08075(1)
	U_{eq} (Å^2)	0.0065(1)	0.00492(6)	0.00671(6)	0.00527(5)	0.00541(6)	0.00529(8)	0.0072(1)
Ge1	*x*/*a*	0	0	0	0	0	0	0
(8*f*)	*y*/*b*	0.13181(8)	0.1285(1)	0.1286(2)	0.1291(3)	0.1332(1)	0.1304(1)	0.1345(1)
	z/*c*	0.02868(3)	0.03066(2)	0.03042(3)	0.03023(2)	0.02798(3)	0.02917(4)	0.02720(5)
	U_{eq} (Å^2)	0.0073(2)	0.0063(1)	0.0084(1)	0.0065(1)	0.0063(1)	0.0062(1)	0.0086(2)
Ge2	*x*/*a*	0	0	0	0	0	0	0
(8*f*)	*y*/*b*	0.11933(8)	0.1217(1)	0.1213(2)	0.1213(3)	0.1185(1)	0.1205(1)	0.1177(1)
	z/*c*	0.45753(3)	0.46255(2)	0.46216(3)	0.46146(2)	0.45619(3)	0.46051(4)	0.45459(5)
	U_{eq} (Å^2)	0.0083(2)	0.0075(1)	0.0089(1)	0.0077(1)	0.0076(1)	0.0082(2)	0.0097(2)
Ge3	*x*/*a*	0	0	0	0	0	0	0
(8*f*)	*y*/*b*	0.40519(8)	0.40516(7)	0.40475(8)	0.40492(8)	0.40524(8)	0.4047(1)	0.4052(1)
	z/*c*	0.19344(3)	0.19462(3)	0.19441(3)	0.19422(3)	0.19305(3)	0.19403(4)	0.19299(5)
	U_{eq} (Å^2)	0.0073(2)	0.0076(1)	0.0089(2)	0.0072(2)	0.0062(1)	0.0048(1)	0.0085(2)
Ge4	*x*/*a*	0	0	0	0	0	0	0
(8*f*)	*y*/*b*	0.34733(8)	0.34524(7)	0.34608(8)	0.34617(8)	0.34763(8)	0.3476(1)	0.3484(1)
	z/*c*	0.30752(3)	0.30553(3)	0.30572(3)	0.30599(3)	0.30810(3)	0.30685(4)	0.30862(5)
	U_{eq} (Å^2)	0.0075(2)	0.0077(1)	0.0086(2)	0.0069(2)	0.0067(1)	0.0060(2)	0.0079(2)
Ge5	*x*/*a*	0.27688(6)	0.27767(5)	0.27735(4)	0.27729(4)	0.27700(5)	0.27568(7)	0.27669(8)
(16*g*)	*y*/*b*	0.12631(5)	0.12531(8)	0.12540(1)	0.1254(2)	0.12658(7)	0.12614(7)	0.1267(1)
	z/*c*	0.19308(2)	0.19461(2)	0.19442(2)	0.19416(2)	0.19259(2)	0.19379(2)	0.19237(3)
	U_{eq} (Å^2)	0.0073(1)	0.00764(8)	0.00864(9)	0.00686(8)	0.00625(9)	0.0055(1)	0.0082(2)
Pd	*x*/*a*	0	0	0	0	0	0	0
(8*f*)	*y*/*b*	0.12736(5)	0.12526(6)	0.12555(6)	0.12572(6)	0.12762(6)	0.12666(7)	0.12826(9)
	z/*c*	0.14223(2)	0.14568(2)	0.14496(2)	0.14453(2)	0.14153(2)	0.14132(2)	0.14062(3)
	U_{eq} (Å^2)	0.0060(1)	0.00664(8)	0.00765(9)	0.00585(8)	0.00504(8)	0.0039(1)	0.0068(2)

straightforward and the following possible space groups were suggested for the *C*-centered monoclinic cell: *C*2 (no. 5), *Cm* (no. 8) and *C*2/*m* (no. 12). The lowest combined figure of merit was associated with the only centrosymmetric *C*2/*m* space group. These data strongly hint that the studied crystal is isostructural with the monoclinic *mS*36-La_2AlGe_6 prototype. A preliminary structural model, obtained by direct methods as implemented in WinGx,[35] contained 1 La, 5 Ge and 1 Pd, giving the correct La_2PdGe_6 composition. Nevertheless, the isotropic thermal parameter values were not coherent for the different types of atoms and three additional intense peaks close to some of the Ge-positions were present in the difference Fourier maps at a distance of ~0.05 nm. The latter three sites have no physical sense if completely occupied and therefore, the sum of occupations for each pair of very close Ge-sites was restrained to be unity in further cycles of least squares refinement. However, the refinement sticks at R_1/wR_2 of 0.05/0.17 with a noisy Fourier map give unreasonable thermal parameters when anisotropically refined. Even less chemically sound structural models were obtained with the possible non-centrosymmetric *C*2 and *Cm* space groups. At this point, more careful analysis of diffraction spots in reciprocal space was performed with RLATT and CELL_NOW.[36] In fact, a regular spatial distribution of extra-peaks was revealed with respect to those associated with the *mS*36-like monoclinic cell. All of them could be satisfactorily indexed with a twice as big monoclinic base centered unit cell with $a \sim 8.2$ Å, $b \sim 8.4$ Å, $c \sim 22.6$ Å, and $\beta \sim 100.5°$. The structural model deduced in the *C*2/*m* space group by the charge-flipping algorithm[30] became less disordered, since it contains only one partially occupied Ge position capping the distorted corrugated Ge fragment.[2] Even if Ge-rich compounds are frequently off-stoichiometric or disordered,[1] residuals remain unsatisfactory (0.09/0.14) with senseless anisotropic thermal parameters. For this reason, more attention was dedicated to the indexing procedure. According to a detailed output of CELL_NOW, one of the possible interpretations of the observed diffraction peak distribution is considering them originating from different domains of a non-merohedrically twinned crystal. In this case, the metric of the single domain remains the same as for the *mS*36 model. All the extra-peaks, instead, are due to the presence of the second domain, related to the first one by a 180° rotation twin law $\begin{pmatrix} 1 & 0 & 0 \\ 0 & -1 & 0 \\ -1/2 & 0 & -1 \end{pmatrix}$.

Consequently, the collected dataset was re-integrated assuming the presence of two domains and the *hkl*5 file for refinement was prepared by TWINABS.[36] After that, excellent residuals were obtained (see Table 5) for the ordered La_2PdGe_6 model with the *mS*36-type structure. At the final cycles, this model was refined with anisotropic thermal displacement parameters for all atom sites. The refined fractional contribution *k* of the second domain is *ca*. 0.4.

The orientation of twin domains and the corresponding reciprocal plots of the completely overlapped and non-overlapped *hkl* zones are shown in Fig. 3. Keeping in mind the twin law, it becomes clear that only reflections with $h = 2n$ are affected by the twinning (*i.e.* they are completely overlapped). Considering also the presence of the only $h + k = 2n$ reflections for the *C*-centered lattice, it is revealed that half of all measured intensities are affected by twinning. The intensity difference between overlapped/non-overlapped reflections is evident from the corresponding precession photos of the *h*2*l* and *h*1*l* zones of reciprocal space shown in Fig. 3.

The crystal structure of Pr_2PdGe_6 isolated from In flux was solved in the same way as for La_2PdGe_6, just described. Its structure turned out to be monoclinic *mS*36, with the same twinning law and with a similar volume ratio to the twinned domains (see Table 2 for more details).

The unit cell volumes of the studied compounds were plotted as a function of the trivalent rare earth metal radii[37] (see Fig. 4). The monoclinic cell volume was doubled in order to compare the different related structures.[2] Only the lattice parameters obtained from single crystal X-ray diffraction were considered.

In agreement with the lanthanide contraction, a linear decreasing trend is observed, suggesting a similar chemical bonding scenario for all the studied germanides. The literature data on Dy_2PdGe_6 [14] fit quite well with the general trend. The most significant deviation is observed for Yb_2PdGe_6; this result is in good agreement with a recent magnetic investigation[8] revealing for Yb a behavior typical of dynamic intermediate valence systems.

Table 5 Atomic coordinates and equivalent isotropic displacement parameters (Å^2) for the La_2PdGe_6 and Pr_2PdGe_6 single crystals obtained by flux synthesis

R_2PdGe_6 analogue	Atomic param.	R (8*j*)	Ge1 (4*i*)	Ge2 (4*i*)	Ge3 (4*i*)	Ge4 (4*i*)	Ge5 (8*j*)	Pd (4*i*)
R = La	*x*/*a*	0.0840(1)	0.1438(3)	0.3585(3)	0.0577(2)	0.4970(2)	0.2773(3)	0.1985(2)
	y/*b*	0.24980(6)	0	0	0	0	0.22206(8)	0
	z/*c*	0.33354(3)	0.5622(1)	0.4281(1)	0.1097(1)	0.1093(1)	0.10943(6)	0.79356(6)
	U_{eq} (Å^2)	0.0045(1)	0.0058(2)	0.0071(2)	0.0092(4)	0.0090(4)	0.0083(2)	0.0064(2)
R = Pr	*x*/*a*	0.0832(3)	0.1453(6)	0.3580(6)	0.0573(3)	0.4981(3)	0.2778(4)	0.1979(2)
	y/*b*	0.24962(7)	0	0	0	0	0.2227(1)	0
	z/*c*	0.33491(4)	0.5609(2)	0.4243(1)	0.1115(2)	0.1112(2)	0.11130(9)	0.7899(1)
	U_{eq} (Å^2)	0.0047(2)	0.0057(3)	0.0075(3)	0.0068(5)	0.0070(5)	0.0066(2)	0.0056(2)

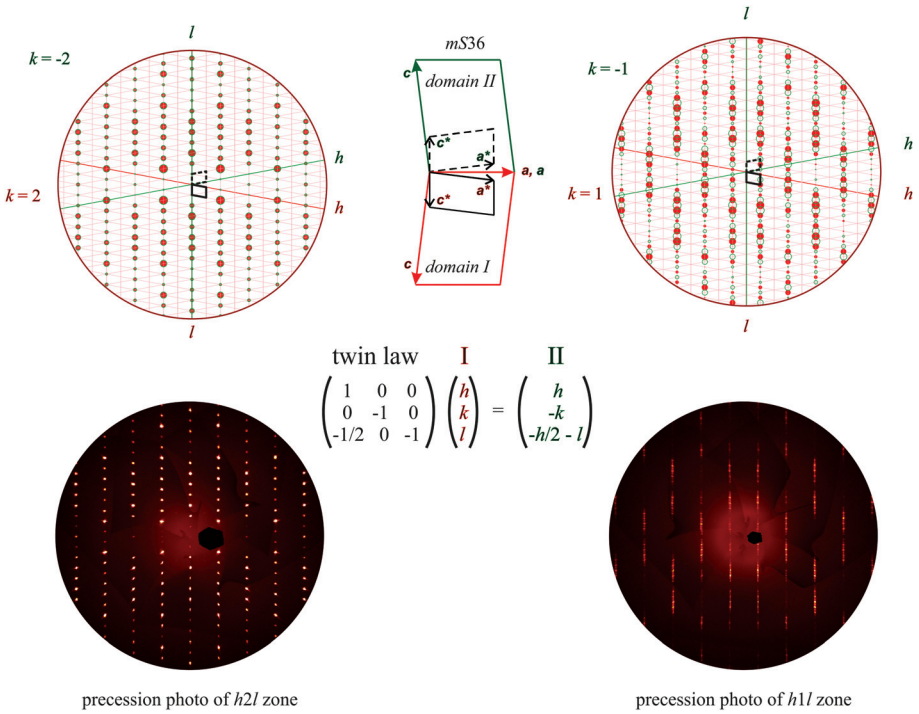

Fig. 3 Upper part: Reciprocal orientation of twin domains together with theoretical reciprocal plots of *h2l* (totally overlapped) and *h1l* (non-overlapped) zones generated by XPREP.[20] Colors of domains I (red) and II (green) are the same as those of the corresponding *hkl* reflections. For clarity, relationships between direct/reciprocal lattice vector lengths are not considered. Lower part: Experimental precession photos of *h2l* and *h1l* zones.

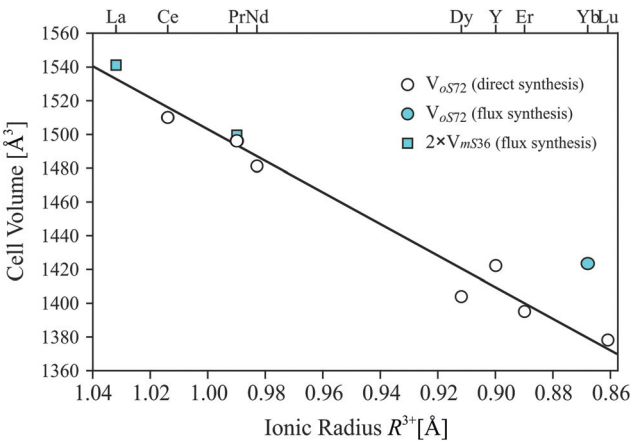

Fig. 4 Normalized cell volumes (from single crystal data) of R_2PdGe_6 compounds as a function of the R^{3+} ionic radius. The cell volume of Dy_2PdGe_6 was taken as per ref. 14.

The crystal structure of the R_2PdGe_6 (R = Sm, Gd, Tb, Ho and Tm) compounds was not studied by single crystal X-ray diffraction. The powder diffraction patterns, recorded on the corresponding samples, can be satisfactorily indexed to both *oS*72 and *mS*36 structures. However, considering the results obtained on the directly synthesized samples with early and late rare earth metals, it is reasonable to suggest that under the same conditions even the abovementioned R_2PdGe_6 phases are of the *oS*72-$Ce_2(Ga_{0.1}Ge_{0.9})_7$ type.

A similar rationalization could not be made for the crystal structure of the 2 : 1 : 6 germanides synthesized by the flux method since for Pr_2PdGe_6 a different structure was stabilized, instead for Yb_2PdGe_6 the same orthorhombic modification is formed.

3.3 From R_2PdGe_6 to R_2MGe_6 compounds: crystallochemical and DFT analyses targeting the correct structural model

From the results described above, it is clear that the *oS*18-Ce_2CuGe_6 structure is never realized in the R_2PdGe_6 series. Within this family, direct synthesis always produces compounds belonging to the *oS*72-$Ce_2(Ga_{0.1}Ge_{0.9})_7$ structure type, except for La_2PdGe_6, whose structure under these conditions was not definitely confirmed. The In-flux synthetic route used in this study gave origin to *mS*36-La_2AlGe_6 twinned crystals of La_2PdGe_6 and Pr_2PdGe_6, whereas Yb_2PdGe_6 crystals grown from the same metal solvent are orthorhombic *oS*72. These results are coherent with recent structural studies on 2 : 1 : 6 germanides assigning to them the *oS*72[7,9,14,15] or the *mS*36 model[17] instead of the previously proposed *oS*18.

In view of the following discussion it is convenient to distribute all the known 2 : 1 : 6 models within a concise scheme (Bärnighausen tree) starting from the *oS*20-$SmNiGe_3$ aristotype. When considering the vacancy ordering phenomenon[16,38,39] causing symmetry reduction, each structural model finds its location on a separate branch. To capture the

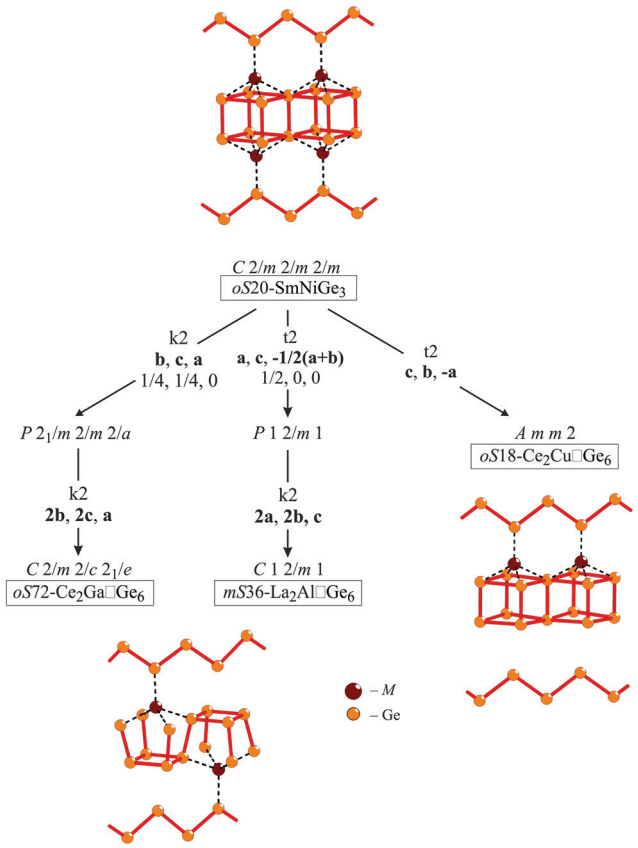

Fig. 5 Bärnighausen tree relating to the $SmNiGe_3$ aristotype and its orthorhombic and monoclinic vacancy variants. The type and indexes of the symmetry reductions are indicated. For clarity, only M–Ge frameworks are shown for each structural model; Ge–Ge contacts are shown in red, M–Ge interactions by a dotted line.

changes taking place, it is sufficient to follow the M–Ge sublattice distortions as depicted in Fig. 5 (R atom positions are negligibly affected by the symmetry reduction).

From the crystal chemical point of view, the *oS*18 model is somewhat suspicious:

- it contains many independent crystallographic Ge sites, not in agreement with the symmetry principle;[40]

- the inhomogeneous vacancy distribution implies that corrugated Ge layers are linked to the zig-zag germanium chains through bridging M atoms only on one side (see Fig. 5).

To corroborate this idea arising from symmetry considerations, the DFT total energy values were calculated for La_2PdGe_6 and Y_2PdGe_6 with the *oS*18, *oS*72 and *mS*36 structures. The structural data available in the literature or obtained during this work were used as the starting point for geometric relaxation. In the case of Y_2PdGe_6, for which the *mS*36 model has never been reported, the cell dimensions and atomic positions of the La-analogue were chosen. The choice of these rare earths allows avoiding the presence of highly correlated electrons lying in partially filled *f* states. The relaxed structures, obtained at the end of the variable-cell calculations, showed lattice constants about 2% larger with respect to the literature data and results presented in this work, as expected when using the PBE functional (see Table 6).

On the basis of the obtained results the *oS*18 structural model is the worst: its total energy is higher by 0.063 eV per atom for La_2PdGe_6 and by 0.066 eV per atom in the case of Y_2PdGe_6 with respect to both *oS*72 and *mS*36 models.

Calculations for the *oS*18 and *oS*72 models were performed on other La_2MGe_6 analogues (M = Pt, Cu, Ag and Au). As can be seen from the plot shown in Fig. 6, the highest energy value corresponds always to the *oS*18 model (ΔE(eV per at) = $E_{oS72} - E_{oS18}$, is always negative).

The *mS*36 model was not considered for energy calculations of La_2MGe_6 because the results on La_2PdGe_6 and Y_2PdGe_6 (Table 6) do not show any energy difference between *oS*72 and *mS*36. In fact, they can be considered as two different polytypes of 2 : 1 : 6 composition. They both consist of geometrically equivalent layers of defective $BaAl_4$ (of R□MGe_2 composition),

Table 6 Experimental and calculated parameters for R_2PdGe_6 (R = La and Y) in the *oS*18, *oS*72 and *mS*36 modifications. If not specified, data were obtained in this work

		Experimental			Calculated		
Compound		*oS*18	*oS*72	*mS*36	*oS*18	*oS*72	*mS*36
Y_2PdGe_6	*a* (Å)	4.0790(4)	8.1703(5)		4.1502	8.3117	8.2181
	b (Å)	4.0168(5)	8.0451(5)		4.0802	8.2239	8.3140
	c (Å)	21.525(2)	21.558(2)		22.212	21.857	11.123
	β (°)						100.5
	V (Å^3)	352.7(1)	1417.1(2)		376.14	1494.0	747.16
	Energy (eV per atom)				−691.647	−691.713	−691.713
	Ref.	3					
La_2PdGe_6	*a* (Å)	4.2117(3)	8.430(1)	8.2163(8)	4.2914	8.5552	8.3910
	b (Å)	4.1100(3)	8.2180(7)	8.4161(9)	4.1893	8.3902	8.5554
	c (Å)	22.265(5)	22.192(3)	11.294(1)	22.913	22.642	11.515
	β (°)			100.5(1)			100.5
	V (Å^3)	385.4(1)	1537.4(4)	768.0(1)	411.92	1625.2	812.81
	Energy (eV per atom)				−721.181	−721.244	−721.244
	Ref.	3	4				

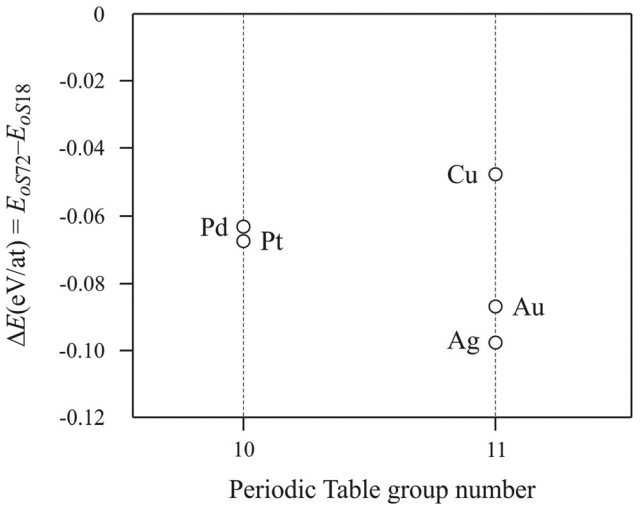

Fig. 6 ΔE *vs.* nature of late transition element M for La_2MGe_6.

AlB_2 and α-Po type slabs stacked linearly along the *c* direction.[2,41] These layers are also energetically equivalent, and consequently no strong preference for one of the polytypes can be envisaged. Frequently, the structure of such compounds is sensitive to the crystallization conditions and small fluctuations of these may reverse the energetic preferences and at the same time give origin to stacking faults, twinnings or non-periodic structures; as an example the families of SiC, ZnS, CdI_2, micas, *etc*. can be cited.[42]

These findings do not preclude the possibility that new polytypes exist for this numerous group of compounds. One can suppose that modulated structures may form within this family. The non-periodicity could arise from a vacancy ordering or Ge covalent fragment distortions with a periodicity different from that of lattice. This phenomenon was addressed in a recent paper on structurally related germanides.[43]

Some more aspects associated with the symmetry reduction scheme can be highlighted. The symmetry reduction path conducive to the *mS*36 model contains a *translationengleiche* transformation of index 2 that is in perfect agreement with the fact that non-merohedral two domain twins are formed. The presence of *klassengleiche* relations, instead, should be at the origin of antiphase domains in both *oS*72 and *mS*36 polytypes. These domains are not detectable by conventional X-ray diffraction techniques; however, the quality and dimensions of single crystals obtained by the flux method are well promising for further transmission electron microscopic investigations to achieve this goal.

It remains, however, unclear if the *oS*20 aristotype has any physical meaning. Further investigations should be performed aiming to clarify if elevated temperature/pressure conditions may stabilize the hypothetical *oS*20-$RPdGe_3$. If yes, the found non-merohedral twins have been developed by a phase transition in the solid state. Otherwise, their formation took place during the growth of the crystal.

4. Conclusions

The R_2PdGe_6 series of compounds was targeted with the aim to elucidate more on the formation/crystal structure of the R_2MGe_6 family (R = rare earth metal, M = another metal), combining the experimental results with structure analysis and energy calculations. This study was motivated by the controversial and sometimes erroneous structural data available for the title compounds, possibly also affecting the interpretation of the numerous magnetic measurements performed by several authors.

The R_2PdGe_6 phase was detected in all samples prepared by direct synthesis, except for R = Sc and Eu.

Single crystal X-ray analyses conducted on several representative samples (R = Y, Ce, Pr, Nd, Er and Lu) indicated that *oS*72-$Ce_2(Ga_{0.1}Ge_{0.9})_7$ is the correct structural model, as previously reported for the Dy and Yb analogues. The same crystal structure is suggested for R = Sm, Gd, Tb, Ho and Tm on the basis of powder X-ray diffraction measurements and behavior regularities along the rare-earth series.

Different annealing treatments along with thermal analysis investigations were performed with the aim to obtain good crystals or a sufficiently high yield of La_2PdGe_6; the obtained results suggest that this is a metastable phase likely to form in a small amount during slow cooling treatments.

Therefore, the flux synthesis, able to stabilize metastable phases, was explored, using In as a metal solvent. The good quality La_2PdGe_6 crystals obtained after optimizing this method are non-merohedrally twins of the *mS*36-La_2AlGe_6 structure. Monoclinic twins of two equally big domains of the same morphology were obtained for the flux-synthesized Pr_2PdGe_6 compound. This result suggests that also La_2PdGe_6 obtained from direct synthesis might be of the *oS*72 orthorhombic structure. Instead, for the heavy rare earth representative Yb_2PdGe_6 the flux does not stabilize the monoclinic structure, and the *oS*72 model remains the correct one.

Taking into account the considerable amount of data on 2 : 1 : 6 germanides, some structure-rationalizing idea was pursued. Considering the vacancy ordering phenomenon to be the key-factor for structural changes, a compact Bärnighausen tree was constructed, with rigorous group–subgroup relations between the *oS*20-$SmNiGe_3$ aristotype and the three possible derivatives *oS*72, *mS*36 and *oS*18: their structural models are localized on separate branches of the tree, representing different symmetry reduction paths. The presence of a t2 reduction step on the path bringing to the *mS*36 model is coherent with the formation of twinned crystals.

Both from our experience and literature data,[44,45] binary and ternary germanides are particularly prone to geminate, and this possibility should be carefully investigated during structural solution. For this reason these phases are also suitable for studies targeted to better understand the origin, formation conditions and type of twinning in intermetallics. At present, we are further studying twinned crystals of germanides, where twinning seems to be related to vacancy ordering phenomena.

The same phenomena can lead to modulated structures, as already found for binary RGe_{2-x} [46] and ternary germanides,[46] representing another reason for interest in the studied compounds.

From the presented symmetry reduction scheme the symmetry discrepancy became obvious between the *oS*18 (2nd order derivative of the aristotype) and both the *oS*72 and *mS*36 models (4th order derivatives), highlighting the poor crystal chemical reliability of the structure mostly reported in the literature and already corrected for several R_2MGe_6 compounds.

Aiming to confirm this idea and to discard energetically less probable modifications, DFT total energy calculations were performed for R_2PdGe_6 (R = Y and La) in the three above-mentioned structural models, and for La_2MGe_6 (M = Pt, Cu, Ag and Au) in the *oS*18 and *oS*72 modifications. Structure optimization was performed for all calculations. Considering the total energy highest values as well as the crystallochemical factors, the *oS*18-Ce_2CuGe_6 model is less probable. It was also concluded that the *oS*72 and *mS*36 models, containing geometrically equivalent fragments, are energetically equivalent polytypes. In fact, they are sensitive to the crystallization conditions, as it became clear from the results of the flux synthesis. This approach turned out to be an effective alternative method to prepare these compounds.

The mostly structural study presented in this paper constitutes a good and essential basis for further investigations concerning the chemical bonding for R_2MGe_6, which is already one of the objects of our research work.

Conflicts of interest

There are no conflicts to declare.

Acknowledgements

The authors thank D. Ceresoli (CNR-ISTM, Milano) for support in DFT calculations. DMP acknowledges the Ministry of Education and Science of Russia (grant 14.B25.31.0005).

References

1 P. Villars and K. Cenzual, *Pearson's Crystal Data*, ASM International, Ohio, USA, Release 2016/17.
2 P. Solokha, S. De Negri, D. M. Proserpio, V. A. Blatov and A. Saccone, *Inorg. Chem.*, 2015, **54**, 2411.
3 O. L. Sologub, K. Hiebl, P. Rogl and O. I. Bodak, *J. Alloys Compd.*, 1995, **227**, 37.
4 M. Konyk, L. Romaka, D. Gignoux, D. Fruchart, O. Bodaka and Yu. Gorelenko, *J. Alloys Compd.*, 2005, **398**, 8.
5 K. Shigetoh, D. Hirata, M. A. Avila and T. Takabatake, *J. Alloys Compd.*, 2005, **403**, 15.
6 D. Kaczorowski, M. Konyk, A. Szytu1a, L. Romaka and O. Bodak, *Solid State Sci.*, 2008, **10**, 1891.
7 R. Wawryk, R. Tróc and A. V. Gribanov, *J. Alloys Compd.*, 2012, **520**, 255.
8 D. Kaczorowski, M. Konyk and L. Romaka, *J. Alloys Compd.*, 2012, **526**, 22.
9 D. Kaczorowski, A. V. Gribanov, P. Rogl and S. F. Dunaev, *J. Alloys Compd.*, 2016, **685**, 957.
10 M. B. Konyk, L. P. Romaka, Yu. K. Gorelenko and O. I. Bodak, *J. Alloys Compd.*, 2000, **311**, 120.
11 V. V. Pavlyuk, V. K. Pecharskii and O. I. Bodak, *Kristallografiya*, 1988, **33**, 43.
12 A. Stetskiv, R. Misztal and V. V. Pavlyuk, *Acta Crystallogr., Sect. C: Cryst. Struct. Commun.*, 2012, **68**, i60.
13 C. Rizzoli, O. Sologub and P. Salamakha, *J. Alloys Compd.*, 2003, **351**, L10.
14 A. Gribanov, S. Safronov, E. Murashova and Y. Seropegin, *J. Alloys Compd.*, 2012, **542**, 28.
15 M. L. Fornasini, P. Manfrinetti and A. Palenzona, *Z. Kristallogr.*, 2002, **217 NCS**, 173.
16 S. De Negri, P. Solokha, M. Skrobańska, D. M. Proserpio and A. Saccone, *J. Solid State Chem.*, 2014, **218**, 184.
17 S. C. Peter, U. Subbarao, S. Sarkar, G. Vaitheeswaran, A. Svane and M. G. Kanatzidis, *J. Alloys Compd.*, 2014, **589**, 405.
18 J. T. Zhao, K. Cenzual and E. Parthè, *Acta Crystallogr., Sect. C: Cryst. Struct. Commun.*, 1991, **47**, 1777.
19 Yu. Grin, in *Modern Perspectives in Inorganic Crystal Chemistry*, ed. E. Parthè, Kluwer Academic Publishers, Dordrecht, the Netherlands, 1992, p. 77.
20 Bruker, *APEX2, SAINT-Plus, XPREP, SADABS and TWINABS*, Bruker AXS Inc., Madison, Wisconsin, USA, 2014.
21 W. Kraus and G. Nolze, *J. Appl. Crystallogr.*, 1996, **29**, 301.
22 P. Giannozzi, S. Baroni, N. Bonini, M. Calandra, R. Car, C. Cavazzoni, D. Ceresoli, G. L. Chiarotti, M. Cococcioni, I. Dabo, A. Dal Corso, S. de Gironcoli, S. Fabris, G. Fratesi, R. Gebauer, U. Gerstmann, C. Gougoussis, A. Kokalj, M. Lazzeri, L. Martin-Samos, N. Marzari, F. Mauri, R. Mazzarello, S. Paolini, A. Pasquarello, L. Paulatto, C. Sbraccia, S. Scandolo, G. Sclauzero, A. P. Seitsonen, A. Smogunov, P. Umari and R. M. Wentzcovitch, *J. Phys.: Condens. Matter*, 2009, **21**, 395502.
23 J. P. Perdew, K. Burke and M. Ernzerhof, *Phys. Rev. Lett.*, 1996, **77**, 3865.
24 D. Vanderbilt, *Phys. Rev. B: Condens. Matter*, 1990, **41**, 7892.
25 GBRV high-throughput pseudopotential, http://physics.rutgers.edu/gbrv, (accessed May 2017).
26 T. B. Massalski, *Binary Alloy Phase Diagrams*, American Society for Metals, Metals Park, Oh 44073, USA, 1990, vol. 2.
27 M. G. Kanatzidis, R. Pöttgen and W. Jeitschko, *Angew. Chem., Int. Ed.*, 2005, **44**, 6996.
28 P. Solokha, R. Freccero, S. De Negri, D. M. Proserpio and A. Saccone, *Struct. Chem.*, 2016, **27**, 1693.
29 J. R. Salvador, J. R. Gour, D. Bilc, S. D. Mahanti and M. G. Kanatzidis, *Inorg. Chem.*, 2004, **43**, 1403.
30 V. Petricek, M. Dusek and L. Palatinus, *Z. Kristallogr.*, 2014, **229**, 345.

31 G. M. Sheldrick, *Acta Crystallogr., Sect. A: Fundam. Crystallogr.*, 2008, **64**, 112–122.
32 L. M. Gelato and E. Parthé, *J. Appl. Crystallogr.*, 1987, **20**, 139.
33 P. Müller, *Crystal structure refinement: a crystallographer's guide to SHELXL*, Oxford University Press, Oxford, UK, 2006.
34 W. Clegg, *Crystal structure analysis: principle and practice*, Oxford University Press, Oxford, UK, 2nd edn, 2009.
35 L. J. Farrugia, *J. Appl. Crystallogr.*, 1999, **32**, 837.
36 Bruker, *APEX2, SAINT-Plus, XPREP, SADABS, CELL_NOW and TWINABS*, Bruker AXS Inc., Madison, Wisconsin, USA, 2014.
37 R. D. Shannon, *Acta Crystallogr.*, 1976, **32**, 751.
38 S. C. Peter, M. Chondroudi, C. D. Malliakas, M. Balasubramanian and M. G. Kanatdidis, *J. Am. Chem. Soc.*, 2011, **133**, 13840.
39 J. Christensen, S. Lidin, B. Malaman and G. Venturini, *Acta Crystallogr., Sect. B: Struct. Sci.*, 2008, **64**, 272.
40 U. Müller, *Symmetry Relationships between Crystal Structures. Applications of Crystallographic Group Theory in Crystal Chemistry*, Oxford University Press, Oxford, UK, 2013.
41 Y. O. Tokaychuk, Y. E. Filinchuk, A. O. Fedorchuk, A. Yu. Kozlov and I. R. Mokra, *J. Solid State Chem.*, 2006, **179**, 1323.
42 E. Prince, *International Tables for Crystallography, Vol. C, Mathematical, physical and chemical tables*, Kluwer Academic Publishers, Dordrecht, 2004.
43 J. Zhang, Y. Liu, C. H. Shek, Y. Wang and S. Bobev, *Dalton Trans.*, 2017, **46**, 9253.
44 S. Budnyk, F. Weitzer, C. Kubata, Y. Prots, L. G. Akselrud, W. Schnelle, K. Hiebl, R. Nesper, F. R. Wagner and Y. Grin, *J. Solid State Chem.*, 2006, **179**, 2329.
45 O. Shcherban, I. Savysyuk, N. Semuso, R. Gladyshevskii and K. Cenzual, *Chem. Met. Alloys*, 2009, **2**, 115.
46 P. H. Tobash, D. Lins and S. Bobev, *Inorg. Chem.*, 2006, **45**, 7286.